Sādhanā (2020)45:186
https://doi.org/10.1007/s12046-020-01423-0

Satellite image based flood classification in urban areas using B-convolutional networks

R BANUPRIYA[1,*] and A RAJIV KANNAN[2]

[1]Department of Computer Science and Engineering, Vidyaa Vikas College of Engineering and Technology, Tiruchengode, India
[2]Department of Computer Science and Engineering, K.S.R. College of Engineering, Tiruchengode, India
e-mail: banurpriya@protonmail.com

MS received 27 January 2020; revised 11 May 2020; accepted 23 June 2020

Abstract. Spatial features with spectral properties enhance the quality of satellite image while mapping complex land cover. These features are integrated with the proposed classification approach for improving classification results. The ultimate objective of this investigation is to provide high-level features to the convolutional neural network (CNN) for mapping flooded regions (before and after) using remote sensing data. Here, boundary-based segmentation is done to recognize the dimensions and scales of objects. Modeling a fully trained Convolutional network is feasible for training a huge amount of data in remote sensing studies. Fine-tuned CNN is utilized with slight modification for attaining classified Landsat images. Classification outcomes and confusion matrix are manipulated using B-CNN are compared with classifiers like SVM, random forest (RF) to compute B-CNN efficiency.

Keywords. CNN; mapping; remote sensing; spatial feature; flood mapping; classification.

1. Introduction

With vast development in the field of satellite imaging and spontaneous observation of earth, there exists a huge factor for cumulating high-resolution satellite images for practical applications [1]. While comparing land cover information, high-level information is measured as sub-image semantic abstractions such as categorizing scenes [2]. Thus, scene classification is a recognition approach to haul out high-level semantic information from high spatial resolution images [3]. Furthermore, prevailing classification approaches are sourced on pixel/object, which does not achieve this task as there is an existence of a semantic gap. As an alternative, it is evaluated as a challenging and open crisis for sensed image classification. Recently, deep learning has turned out to be a novel solution of a traditional approach, like computer visual recognition [4]. It has attained major enhancements towards existing records like object recognition, speech and face detection, action detection, remotely sensed scene classification, semantic segmentation, and nature images classification [5]. To be more specific, CNN is acknowledged as a proficient approach to deal hierarchical abstraction level with provided input data by encoding those input data over various layers [6]. In contrast to conventional classification approaches, DL has attained superior classification performance in remote sensing. Enormous works have been implemented with the conventional CNN model using pre-trained datasets and transformed as a classification model [7–14].

2. Overview

Generally, CNN comprises of fully connected layers and Convolutional layers. A data source is attained from Chennai Flood in the year 2015 as a report provided by the Controller and Auditor General of India (CAG) report. Next, preprocessing is performed by segmenting satellite-based flooded image segmentation. Dimensionality reduction is considered while performing boundaries based segmentation (BOS). CNN based feature extractor extracts higher-level features of flooded scene matching region from a satellite view. For higher-level feature extraction, connected components with higher probability with boundary information (BI) and Bayesian dissimilarity criteria (BDSC) are determined. Finally, pre-trained CNN extracts classified flooded images that provide an accuracy of about 90%.

Data source, Data preprocessing, Boundary based segmentation, High-level features, and Label initialization are the processes to be performed. Data has been collected from the report given by CAG regarding the

*For correspondence
Published online: 21 July 2020

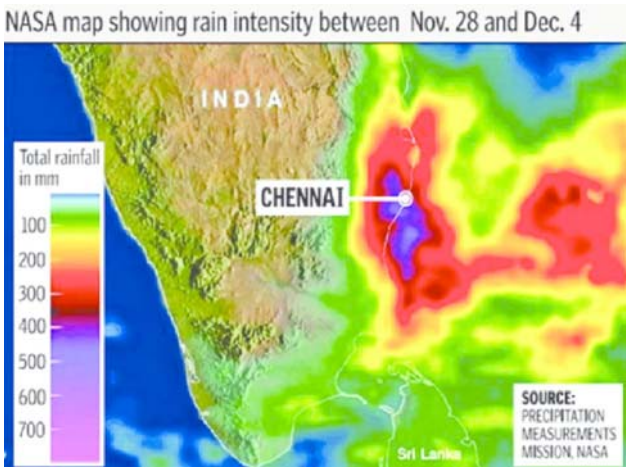

Figure 1. Landsat view of the flooded region.

Chembarambakkam tank between December 2015. Figure 1 depicts the satellite view of the flood-affected regions.

2.1 *B-CNN*

Here, B-CNN is proposed for dealing complexities of higher-level features and nonlinear spatial analysis of higher-level Landsat image

$$a^1 = g\left(F^1 * h^0 + b^1\right) \tag{1}$$

Here, $*$ is convolutional operator, h^0 specifies input Landsat images, F^1 specifies filter of convolution layer, $b^1$is a bias of the convolution layer correspondingly. $g(.)$ specifies the ReLU activation function. a^1 specifies the output feature map of the convolution layer and pooling layer input (i.e., layer two).

With pooling operation, higher-level feature map shrink, however, turns to be more effectual and robust as given in (figure 2)

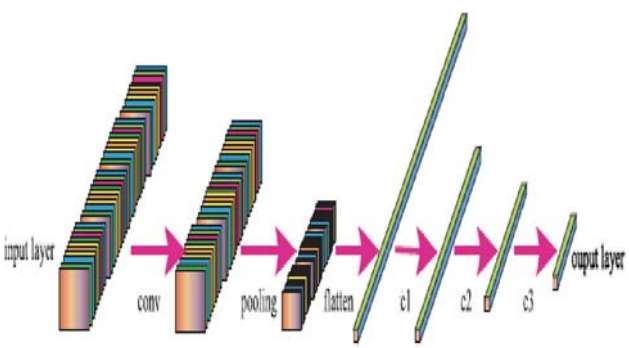

Figure 2. B-CNN architecture.

$$a^2 = g\left(down\left(a^1\right)\right) \tag{2}$$

where $down(\cdot)$ specifies max pooling function. $g(\cdot)$ specifies ReLU activation function, a^2 specifies the output pooling layers' feature map. Usually, a fully connected layer can be provided as in

$$a^{l+1} = g\left(W^l a^l + b^l\right) \quad where\ l = 2, 3, 4\ldots \tag{3}$$

where a^l is an input of fully connected layer, $W^l and B^l$ are weights/bias of connected layer correspondingly. $g(.)$ specifies ReLU activation function, a^{l+1} specifies connected layer output. Next, Euclidean distance amongst feature vectors of $\{p_1, p_2\}$ is evaluated. A multiscale image is weighed down with sub-sampling and Gaussian smoothing to images of diverse scales. If $I = \{I_1, I_2, I_3, \ldots, I_M\} \in R^{m*m*d}$, 'M' specified number of images, 'm' image size, 'd' number of channels. Multiscale image is depicted as $\left\{I_i^l\right\}_{l=0}^n, I_i^0 = I_i$, where 'l' is the scale level. Smoothing and sampling in CNN for adjacent levels are done as

$$I_i^{l+1} = G * I_i^l \tag{4}$$

$$I_i^{l+1} = DIMINISH\left(I_i^{l+1}\right) \tag{5}$$

where 'G' is Gaussian co-efficient, * is convolution function, $DIMINISH(\cdot)$ is a sampling function.

$$Z_i^{l,L} = f_L\left(I_i^l\right) \tag{6}$$

where $Z_i^{l,L}$ is the convolutional output of I_i^l on Lth layer; $f(\cdot)$ is pre-trained CNN model, $f_L(\cdot)$ comprises of 'L' convolutional layers.

3. Numerical results and discussion

The simulation was carried out in MATLAB 2018a environment. Online available sources are considered for computation. These images are sufficient to identify the variations of the region before and after a flood. When weight and bias values are provided, true positive values are 747300, a true negative value is 5184600, false-positive value is 621700, and false negative is 0. Samples are partitioned for training and testing. The multi-spectral band of UNOSAT images is depicted in table 1.

Table 2 shows various combinations of Boundary based pixels values, which are defined with three factors like color, scale, and shape. Segmentation based precision values of object boundaries are detected accurately, as shown in figure 3.

The overall accuracy attained by classifying Landsat images is 90.5%. The outcomes demonstrate efficiency against different features offered in the flooded region, as

Table 1. Multi-spectral band.

	Wavelength (micrometers)		
Band num	Landsat 7 ETM+	Landsat 4-5 TM	Landsat MSS
1	0.45–0.52	0.45–0.52	NA
2	0.52–0.60	0.52–0.60	0.5–0.6
3	0.63–0.69	0.63–0.69	0.6–0.7
4	0.77–0.90	0.76–0.90	0.7–0.8
5	1.55–1.75	1.55–1.75	0.8–1.1
6	2.09–2.35	2.08–2.35	NA

Table 2. Evaluation of different combinations of boundary pixel levels.

Landsat images						
Combination of different boundary pixel levels			Scale	Color	Shape	Boundary based objective function
1	1	1	20	0.2	0.2	0.682
1	2	2	20	0.4	0.4	1.082
1	3	3	20	0.6	0.6	1.035
1	4	4	20	0.6	0.6	1.250
1	5	5	20	0.10	0.10	0.966
2	1	2	40	0.4	0.6	1.123
2	2	3	40	0.6	0.6	0.856
2	4	5	40	0.6	0.10	1.155
2	5	1	40	0.10	0.11	1.125
3	1	3	60	0.11	0.5	0.98
3	2	4	60	0.2	0.6	1.16
3	3	5	60	0.6	0.9	0.958
3	4	1	60	0.6	0.12	0.678
3	5	2	60	0.10	0.4	0.713
4	1	1	80	0.1	0.5	0.982

shown in table 3. This phenomenon is significant because of higher-level features attained from Landsat images. Some performance metrics are given below.

$$Accuracy = {}^{(TP+TN)}/_{(TP+FP+TN+FN)} \quad (7)$$

$$True\ positive = {}^{TP}/_{(TP+FN)} \quad (8)$$

$$False\ positive = {}^{FP}/_{(FP+TP)} \quad (9)$$

The classification results are based on extensively utilized boundary-based accuracy, as given above. TP is the amount of precisely hauled out flooded region, TN is the amount of incorrectly hauled out flooded area pixels, FP is the amount of non-flooded water region, FN is the amount of non-extracted non-water region. Figures 4, 5, and 6 show the performance metrics of the proposed model. Parameters

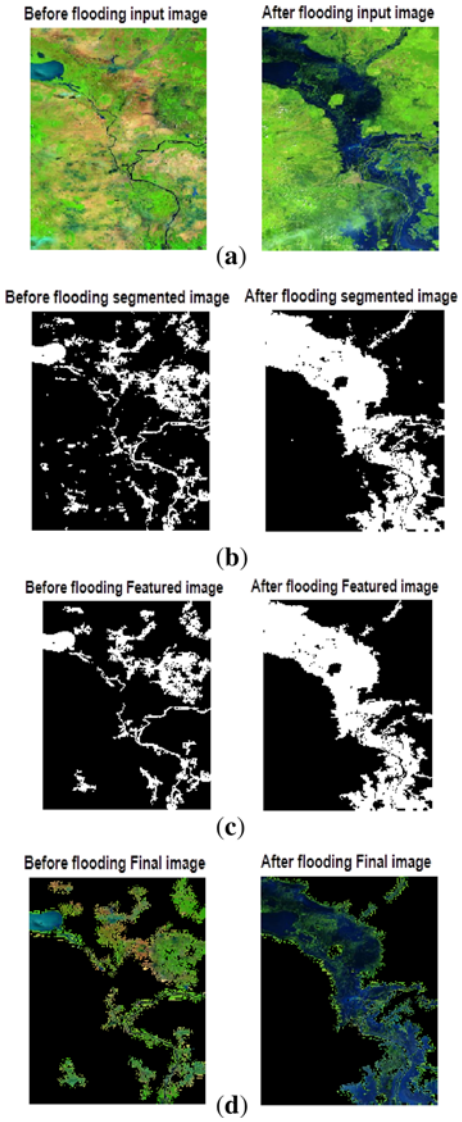

Figure 3. (**a**) Input Landsat image. (**b**) Segmented image. (**c**) High-level feature extracted image. (**d**) Classified Landsat image.

Table 3. Performance metrics comparison of B-CNN with existing models.

Metrics	LDA	CNN	RFF	B-CNN
Accuracy	85.5136	87.0136	88.3036	90.5136
Specificity	84.0927	85.0427	86.8427	89.2927
Precision	48.5873	51.0873	52.3773	54.5873
Recall	93.8000	96.5000	97.7900	100.0000
F-measure	65.7233	66.3733	68.1733	70.6233

of the B-CNN are tabulated in table 3, and its confusion matrix plot is tabulated in table 4.

The accuracy of the proposed B-CNN is 5%, 3.5%, 2.17% higher than LDA, CNN, and RFF, respectively. The

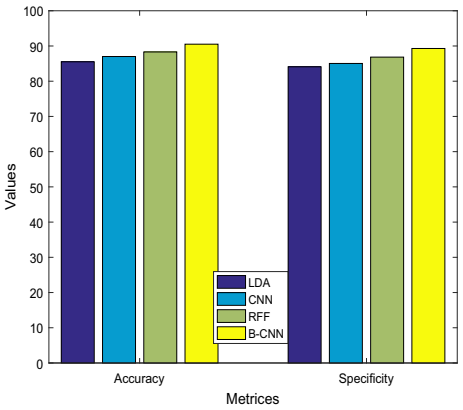

Figure 4. Accuracy and specificity computation.

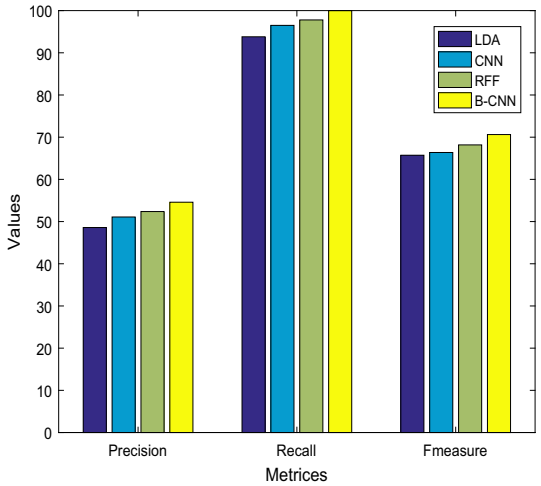

Figure 5. Precision, recall and F-measure computation.

sensitivity of B-CNN is 5.2%, 4.25%, 2.45% higher than LDA, CNN, and RFF, respectively. The precision of B-CNN is 6%, 3.5%, 2.21% higher than LDA, CNN, and RFF, respectively. Recall of the proposed B-CNN is 6.2%, 3.5%, 2.21% higher than LDA, CNN, and RFF, respectively. Similarly, the F-measure of B-CNN is 4.9%, 4.25%, 2.45% higher than LDA, CNN, and RFF, respectively. Henceforth, B-CNN accuracy is higher than LDA, CNN, and RFF can learn to extract features automatically that are more suitable for classification. The drawbacks related to LDA are complex in determining sample size problems, and the discriminative information does not provide any class labels. Similarly, individual CNN does not encode the position and orientation of images for prediction, and RFF shows computational complexity. Henceforth, to overcome the limitation mentioned above, Boundary based segmentation and B-CNN is proposed. This segmentation may consider orientation and position of Landsat images (as edge pixels), and the segmented output is given as input to the classifiers (higher-level spatial feature extraction). This

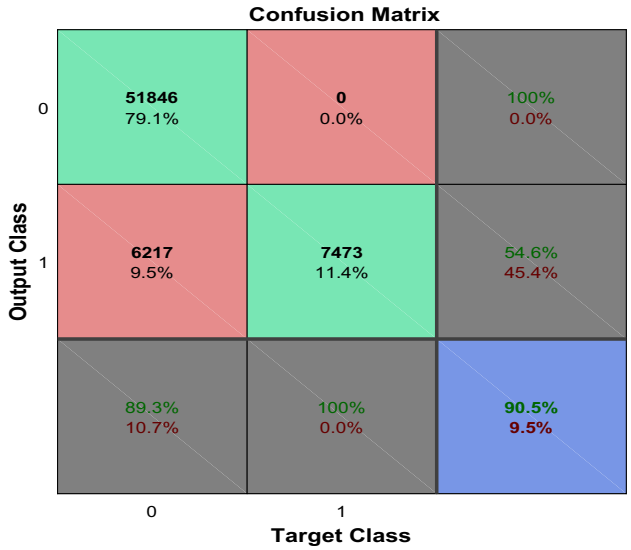

Figure 6. Confusion matrix of various samples.

Table 4. Confusion matrix.

Classes	Producer accuracy	User accuracy
Water bodies	93.07	91.02
Non-water bodies	89.30	90.51
Overall accuracy		90.5

work handles only a small sample size dataset (Meteorological data) for classification purposes. Thereby, it reduces computational complexity.

4. Conclusion

In general, CNN turns to be a more accepted classifier in Landsat image classification, owing to its ability to learn appropriate spatial features. Here, boundary-based segmentation and higher-level features are extracted based on B-CNN to enhance Landsat classification performance for labeled samples provided during training. In specific, B-CNN is trained to enhance the variability of the flooded regions (before and after a flood) with various classes. Subsequently, features extracted through B-CNN are used to train three layers of the CNN classifier. Experimental outcomes provide an accuracy of about 90.51%. In the future, performance can be enhanced by utilizing hybrid models of CNN classifiers.

References

[1] Rujoiu-Mare M R and Mihai B A 2016 Mapping land cover using remote sensing data and GIS techniques: A case study

of Prahova Subcarpathians. *Procedia Environ. Sci.* 32: 244–255

[2] Bian X, Chen C, Tian L and Du Q 2017 Fusing local and global features for high-resolution scene classification. *IEEE J. Sel. Top. Appl. Earth Observ. Remote Sens.* 10: 2889–2901

[3] Huang L, Chen C, Li W and Du Q 2016 Remote sensing image scene classification using multiscale completed local binary patterns and Fisher vectors. *Remote Sens.* 8: 483–499

[4] Liu Y and Huang C 2018 Scene Classification via Triplet Networks. *IEEE J. Sel. Top. Appl. Earth Observ. Remote Sens.* 11: 220–237

[5] Tuia D, Persello C, and Bruzzone L 2017 Recent advances in domain adaptation for the classification of remote sensing data. *IEEE Geosci. Remote Sens. Mag.* 4: 41–57

[6] Zhong Y, Fei F, Liu Y, Zhao B, Jiao H and Zhang L 2017 SatCNN: satellite image dataset classification using agile convolutional neural networks. *Remote Sens. Lett.* 8: 136–145

[7] Yuan Y, Wan J and Wang Q 2016 Congested scene classification via efficient unsupervised feature learning and density estimation. *Pattern Recogn.* 56: 159–169

[8] Yao X, Han J, Cheng G, Qian X and Guo L 2016 Semantic annotation of high-resolution satellite images via weakly supervised learning. *IEEE Trans. Geosci. Remote Sens.* 54: 3660–3671

[9] Maggiori E, Tarabalka Y, Charpiat G and Alliez P 2017 Convolutional neural networks for large-scale remote sensing image classification. *IEEE Trans. Geosci. Remote Sens.* 55: 645–657

[10] Paisitkriangkrai S, Sherrah J, Janney P and Van Den Hengel A 2016 Semantic labelling of aerial and satellite imagery *IEEE J. Sel. Top. Appl. Earth Obs. Remote Sens.* 9: 2868–2881

[11] Prajoona V, Sriramakrishnan P, Sridhar S, Charlyn Pushpa Latha G, Priya A, Ramkumar S, Robert Singh A and Rajendran T 2020 Knowledge based fuzzy c-means method for rapid brain tissues segmentation of magnetic resonance imaging scans with CUDA enabled GPU machine. *J. Ambient Intell. Hum. Comput.* 11: 1–14

[12] Rajendran T, Sridhar K P, Manimurugan S and Deepa S 2019 Recent innovations in soft computing applications. *Curr. Signal Transduct. Ther.* 14: 129–130

[13] Rajendran T, Sridhar K P, Manimurugan S and Deepa S 2019 Advanced algorithms for medical image processing. *Open Biomed. Eng. J.* 13: 102.

[14] Hariraj V, Khairunizam W, Vikneswaran V, Ibrahim Z, Shahriman A B, Zuradzman M R, Rajendran T and Sathiyasheelan R 2018 Fuzzy multi-layer SVM classification of breast cancer mammogram images. *Int. J. Mech. Eng. Technol.* 9: 1281–1299